Delinkage of Metal Surface Saturation Concentration and Micellization in Corrosion Inhibition

Yi He,[*] Shuai Ren,[*] Xi Wang,[*] David Young,[*] Marc Singer,[‡,] Zineb Belarbi,[*] Maalek Mohamed-Saïd,[**] Sheyla Camperos,[***] Md Rubel Khan,[****] and Katherine Cimatu[****]*

Long-distance transmission of oil is usually performed in large-diameter steel pipelines, where water present therein may cause severe internal corrosion. An effective method of mitigating such corrosion is to inject organic corrosion inhibitors (CIs). Their surface adsorption, via heteroatom functionalities, can markedly enhance the corrosion resistance of metals. In this study, three CI model compounds with different head groups but the same alkyl tail length (-$C_{14}H_{29}$), specifically tetradecyltetrahydropyrimidinium (THP-C14), tetradecylphosphate ester (PE-C14), and tetradecylimidazolinium (IMID-C14), were synthesized, their purities being determined using nuclear magnetic resonance spectroscopy. The critical micelle concentrations (CMCs) of each compound were measured using surface tensiometry (Du Noüy ring) and fluorescence spectroscopy techniques, with differences being found between these indirect and direct methods. In addition, linear polarization resistance was used to determine inhibition efficiencies (IEs) for carbon steel immersed in a 5 wt% NaCl electrolyte saturated with CO_2. CI surface saturation concentrations, with maximum IEs, were compared with the determined CMCs. Excellent IEs were observed at concentrations of THP-C14, PE-C14, and IMID-C14 which do not correspond with their CMCs, the differences involved being significantly greater than what was previously reported for tetradecylbenzyldimethylammonium (BDA-C14). These results demonstrate that there is no direct link between CMC and metal surface saturation/corrosion IE that can be made on a generalized basis for the different head groups but with the same tail length CI, indicating that the selection of the appropriate CI concentration for an industrial application should not be based on CMC alone.

KEY WORDS: CO_2 corrosion, corrosion inhibitors, critical micelle concentrations, inhibition efficiency, micellization, surface saturation concentration

INTRODUCTION

In the oil and gas industry, long-distance transportation of petroleum and related products is usually performed in large-diameter carbon steel pipelines. Water present with the oil, along with corrosive species such as CO_2, H_2S, and organic acids, causes severe corrosion of the inner pipe walls.[1] An effective method of controlling corrosion is to continuously inject corrosion inhibitors (CIs) into pipelines conveying oil-water mixtures. As corrosion occurs on water-wetted metal surfaces, CI molecules form protective films which retard electrochemical reaction rates at the water/metal interface[2] thereby protecting carbon steel pipes against CO_2 ("sweet") corrosion and H_2S ("sour") corrosion.

Most commercial CIs are a complex mixture of several compounds that contain surfactant-type active ingredients, such as imidazolinium, amine, pyrimidinium, phosphate ester, and quaternary ammonium derivatives.[3] The performance of these species as CI model compounds is the focus of intensive studies[4-7] in order to deliver descriptive and predictive inhibition models, as well as inhibitor testing methodologies, for industrial users of these compounds. Adsorption of organic molecules on surfaces through heteroatom functionalities, containing nitrogen, oxygen, sulfur, and/or phosphorus, can markedly change the corrosion resistance properties of metals. Such molecules have a strong tendency to adsorb onto the steel surface and form self-assembled structures.[8-9]

Surfactant-type organic inhibitors are, in some cases, applied based on their critical micelle concentration (CMC) values.[10-11] CMC is an important characteristic of a surfactant. It is defined as the concentration of surfactants above which micelles form and all additional surfactant molecules added to the system aggregate as micelles.[12] As shown in Figure 1, below the CMC, the surfactant molecules will partition between the volume of the liquid and the gas/liquid interface with some free CI molecules dispersed in the aqueous phase. Above the CMC, the gas/liquid interface is assumed fully occupied by CI molecules and further addition of surfactant molecules will tend to participate in the formation of micelles. CMC values have been experimentally determined using several different techniques,[13] two of which were applied in the work reported herein. A typically used measurement technique for surface tension is the Du Noüy ring method, where the maximum pulling force on a ring by the surface is measured.[14] The other technique, fluorescence

Submitted for publication: March 10, 2022. Revised and accepted: May 7, 2022. Preprint available online: May 7, 2022, https://doi.org/10.5006/4086.
‡ Corresponding author. E-mail: singer@ohio.edu.
* Institute for Corrosion and Multiphase Technology, Department of Chemical and Biomolecular Engineering, Ohio University, Athens, Ohio 45701.
** TotalEnergies, CSTJF, Avenue Larribau, F-64018 Pau, France.
*** TotalEnergies, TRTG—TOTAL Research & Technology Gonfreville, BP 27 76 700 Harfleur, France.
**** Department of Chemistry and Biochemistry, Ohio University, Athens, Ohio 45701.

ISSN 0010-9312 (print), 1938-159X (online)

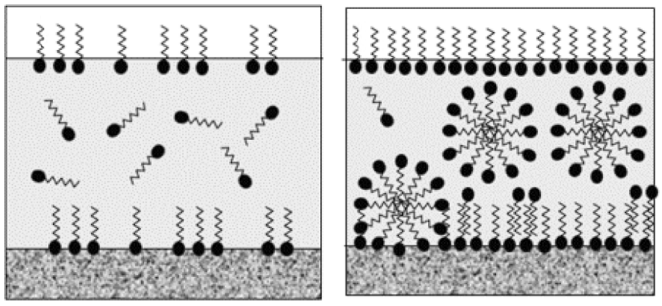

FIGURE 1. *Schematic of scenarios for different concentrations of the inhibitor in solution: (a) below CMC and (b) above CMC.*

spectroscopy (FS), is a method used to exploit the fluorescence properties of a sample to determine concentrations of an analyte in solution.[15] Moradighadi, et al., studied CMC measurements of benzyldimethylalkylammonium (BDA) bromide inhibitor model compounds, possessing the same head group but with different alkyl tail lengths (C6, C8, C10, C12, and C14).[6] Their results demonstrated that surface tension measurements do not always correlate with the formation of micelles. In some cases, the formation of micelles occurred in the same concentration range while in others it happened at much higher concentrations, as determined by FS. However, more work is needed to study whether this observation applies to solely quat-type inhibitors. This will be one of the objectives of the current research.

The metal surface saturation concentration is the minimum concentration that yields the maximum efficiency of a CI. As proposed by Hackerman, et al., CI molecules will continue to adsorb on the metal surface until the metal surface is saturated with the inhibitor, at which the surface saturation concentration is achieved.[16] Any further addition of the inhibitor to the bulk solution should not result in a further significant decrease in the corrosion rate (CR). The amount of the inhibitor added is called the metal surface saturation concentration.[16] According to relevant studies,[10-11,17] when the metal exhibits a maximum decrease of CR, its surface is considered to have reached a state of maximum coverage by inhibitor molecules; increasing the concentration of inhibitor in solution would not lead to an increase in surface coverage and the inhibited CR would remain constant. This statement only applies to bare metal surfaces and not to those subject to precorrosion (i.e., involving the presence of corrosion products or residues). Hypothetically, this scenario can be said to also correspond to a situation where the inhibitor concentration reaches CMC, the inhibitor molecules cannot continue to accumulate at interfaces and instead start forming micelles. Coincidentally, it is common to observe a sharp decrease in CR with the addition of CI but only to a certain concentration, above which no significant change in inhibition efficiency (IE) can be noticed. This concentration, labeled metal surface saturation concentration and corresponding to a condition of maximum IE,[18] has been associated with CMC.[17] Consequently, CMC has been used as an important parameter in determining CI application concentrations and efficiencies. However, recent studies within our laboratory that focused on quaternary ammonium CI model compounds demonstrate that there is no direct link between CMC and surface coverage and, by extension, corrosion IE.[6,19] As stated above, Moradighadi, et al., determined CMC values for a range of BDA bromide inhibitor model compounds.[6] Their study demonstrated that for tetradecylbenzyldimethylalkylammonium inhibitor model compound (BDA-C14), the CMC value was very close to the metal surface saturation concentration (MSSC), while CMC and MSSC of BDA-C12 were dissimilar. Besides, the CMC values of inhibitors with shorter tail lengths (-C6, -C8, and -C10) were not measurable, and thus not comparable with MSSC.

Expanding from the aforementioned research relating to quaternary ammonium species,[6,18-20] the objective of the current work is to further elucidate whether or not the measured CMC values resemble those of MSSC. This is achieved by assessing the performance of different CI model compounds possessing different head groups but with the same alkyl tail length (-$C_{14}H_{29}$). Three CI synthesized model compounds were tetradecyltetrahydropyrimidinium (THP-C14), tetradecylphosphate ester (PE-C14), and tetradecylimidazolinium (IMID-C14). Their purities were determined using nuclear magnetic resonance spectroscopy (NMR). The CMCs of each compound were measured at 25°C using surface tensiometry (Du Noüy ring) and FS techniques. Linear polarization resistance (LPR) measurements were conducted to determine the CR and IEs over a wide range of CI concentrations, from which MSSC and surface coverage (θ) values were extracted. Finally, MSSC, with maximum IE, were compared with the determined CMCs. The CI performance can be assessed by IE, with surface saturation concentration serving as practical dosing guidance. These results are crucial and practical in oil and gas industry applications.

EXPERIMENTAL PROCEDURES

The experimental conditions are selected based on consultation with the industrial sponsor of this project, focusing on inhibitor model compounds possessing different head groups but with the same tail length; specifically THP-C14, PE-C14, and IMID-C14.

2.1 | Synthesis of Corrosion Inhibitor Model Compounds

2.1.1 | Synthesis of 1-Tetradecyl-1,4,5,6-Tetrahydropyrimidinium (THP-C14)

The synthesis reaction for 1-tetradecyl-1,4,5,6-tetrahydropyrimidinium (THP-C14) was depicted in Figure 2. In this reaction, a hydrogen ion (H^+) resides on the more basic N atom in the double bond. This N is more basic because a more stable (resonance stabilized) cation forms after protonation. However, it does not matter which of the two N's in 1,4,5,6-tetrahydropyrimidine is alkylated, as they lead to the identical final product, in which the positive charge is delocalized between the two nitrogen atoms as shown in Figure 2. In this synthesis, acetonitrile (CH_3CN) was chosen as the solvent as it was reported to achieve high amine quaternization rates.[21-22]

The following is the procedure for the synthesis of 1-tetradecyl-1,4,5,6-tetrahydropyrimidinium; this is the same as that used in the synthesis of BDA-C14[19] with tetrahydropyrimidine replacing dimethylbenzylamine:

4.85 g (0.0576 mol) of 1,4,5,6-tetrahydropyrimidine was weighed directly into a 2-necked 250 mL round-bottomed flask. Then, 100 mL acetonitrile was added to the flask. The round-bottomed flask was placed in an appropriately sized heating mantle with four boiling chips added. The condenser and addition funnel containing 15.98 g (0.0576 mol) of 1-bromotetradecane were placed in each flask joint. Cooling water ran through the condenser. The heating mantle, connected to a

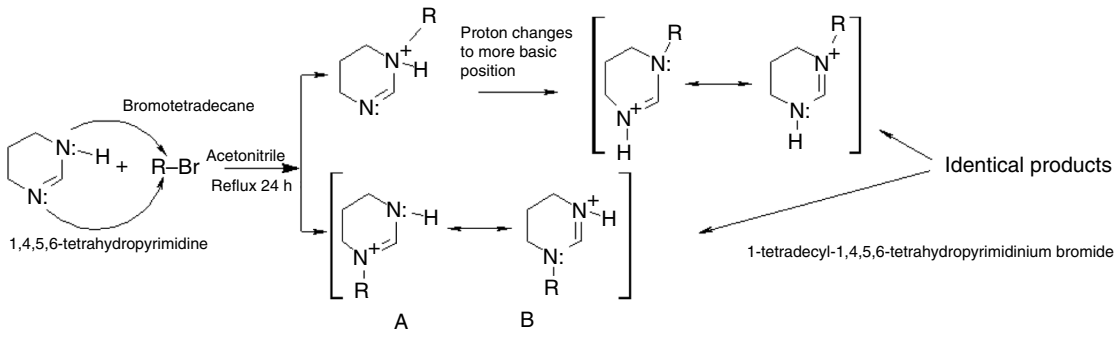

FIGURE 2. *Reaction for the synthesis of THP-C14 inhibitor model compound (R: $C_{14}H_{29}$).*

Variac, was switched on and set to ensure the reaction mixture (acetonitrile/pyrimidine solution) heated to the reflux temperature of ca. 82°C. The 1-bromotetradecane was then added dropwise to the reaction mixture. Reflux was maintained for a further 24 h then the reaction mixture was cooled to room temperature. The acetonitrile was removed by rotary evaporation. The temperature was then increased to 95°C, under vacuum, to drive off any residual volatile species.

2.1.2 | Synthesis of Tetradecylphosphate Ester (PE-C14)

The synthesis of PE-C14 involves esterification to obtain crude products, containing monoester, diester, H_3PO_4, and inorganic phosphates; liquid-liquid extraction to remove H_3PO_4 and inorganic phosphates, and final rotary evaporation to remove diethyl ether introduced in this separation step as a solvent. The net reaction was shown in Figure 3, where ROH is 1-tetradecanol ($C_{14}H_{29}OH$).

The following are the procedures for the synthesis of tetradecylphosphate ester:

42.8 g (0.2 mol) of solid 1-tetradecanol was weighed directly into a 3-necked 250 mL round-bottomed flask. 14.1 g (0.1 mol) phosphorus pentoxide was added and mixed with the 1-tetradecanol. The flask was set in a heating mantle. A condenser, thermometer, and addition funnel were placed in each joint. Water was run through the condenser and the reaction mixture was heated to ca. 80°C, then held at that temperature for 6 h. 1.80 g (0.1 mol) of distilled water was placed in the addition funnel and was added dropwise to the reaction mixture. The reaction continued for 12 h. The product resembled a dark, oily liquid, which yielded a waxy solid upon cooling. This crude product was then treated by liquid-liquid extraction using distilled water and diethyl ether to remove the phosphoric acid, and any inorganic phosphates, using an established procedure.[23] Ether layers were drained using a separatory funnel and then placed in a 500 mL single-necked flask. The ether was removed by rotary evaporation. The temperature was increased to 95°C, under vacuum, to drive off any residual water. The product was an oily liquid which, on cooling, yielded a waxy solid; yield ca. 70%.

2.1.3 | Synthesis of Tetradecylimidazoline (IMID-C14)

The synthesis reaction[24] for the tetradecylimidazoline (IMID-C14) is depicted in Figure 4 (note that the product contains an ethylamine pendent side group). The following represents

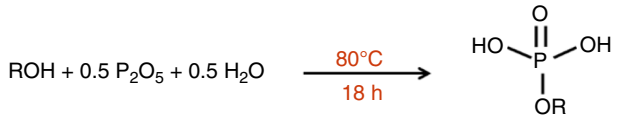

FIGURE 3. *Esterification reaction (R: -$C_{14}H_{29}$).*

the general procedure used for synthesizing the CI model compound IMID-C14:

242.4 g (1 mol) pentadecanoic acid was placed in a 100 mL, 3-neck flask, equipped with a thermocouple, addition funnel, and a Dean-Stark trap. The pentadecanoic acid was heated to 60°C under N_2 for 3 h and then 123.6 g (1.2 mol) of diethylenetriamine (DETA) was added dropwise, rapidly (pentadecanoic acid: DETA was 1:1.2). The resulting mixture color changed to yellow and the temperature was increased to 100°C. The mixture was then heated to ca. 180°C for 3 h while allowing water to collect in the Dean-Stark trap. The resulting mixture was then heated to ca. 230°C for an additional 2 h during which time any further evolved water was collected.

2.2 | Critical Micelle Concentration Measurements

As described by Moradighadi, et al., the procedure for CMC measurements of the inhibitor model compounds was initiated by preparing NaCl solutions with different CI concentrations using series dilution.[19] The surface tension of the solution was measured using a Krüss K20† tensiometer. Before the measurement, the Du Noüy ring was cleaned with deionized water and acetone and then placed above the flame for a few seconds. The procedure was typically stopped when the same/similar surface tension measurements occurred twice.[19] FS measurements were taken using a Fluorolog 3-FLC 21† spectrofluorometer (Horiba Instruments, Edison, NJ). The liquid soluble dye Nile Red[25] (Molecular Probes and Acros) was used as the fluorescence probe in this study, as it demonstrated enhanced fluorescence in a hydrophobic environment, such as when micelles began to form. The Nile Red method has been demonstrated to accurately determine CMC concentrations in comparison to existing data.[26-28] Dimethyl sulfoxide (DMSO, Fisher Scientific) was used as a nonpolar solvent for the Nile Red powder. All of the measurements were performed at least twice to confirm the accuracy of the results.

2.3 | Materials and Chemicals

Carbon steel (UNS G10180[(1)]) (C1018) specimens with a ferritic-pearlitic microstructure (Figure S1) were used for electrochemical measurements. The composition of this carbon steel was shown in Table 1. The electrolyte was prepared by dissolving 100 g sodium chloride (NaCl) in 2 L deionized water

† Trade name.

(1) UNS numbers are listed in *Metals & Alloys in the Unified Numbering System*, published by the Society of Automotive Engineers (SAE International) and cosponsored by ASTM International.

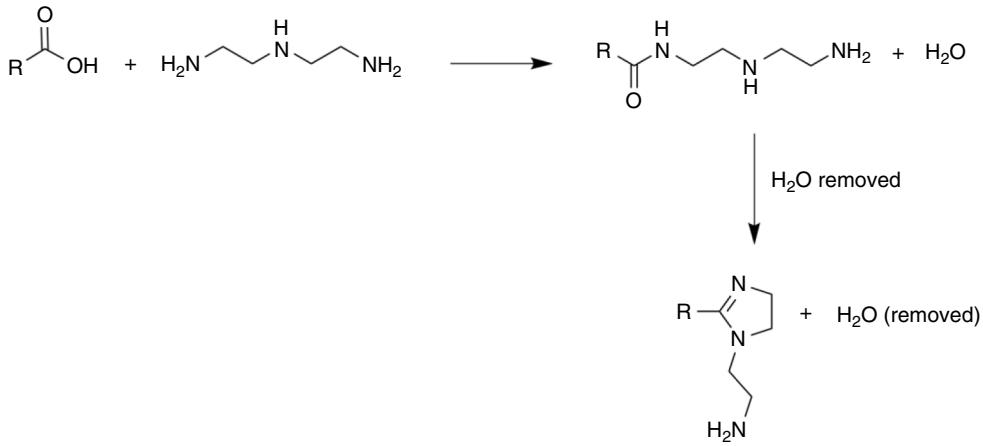

FIGURE 4. *Synthesis of tetradecylimidazoline (IMID-C14) inhibitor model compound (R: -$C_{14}H_{29}$).*

yielding a 5 wt% NaCl electrolyte to simulate exploration and production environments in the oil and gas industry, where the produced water often has a high salt concentration.[29]

2.4 | Electrochemical Measurements

A three-electrode setup (Figure 5) was used to perform electrochemical experiments, with a C1018 rotating cylinder electrode (RCE) as a working electrode, a platinum-coated titanium mesh counter electrode, and an Ag/AgCl (KCl saturated) reference electrode. Before each experiment, the RCE was sequentially polished with 240, 400, and 600 grit silicon carbide abrasive papers, cleaned with isopropanol in an ultrasonic bath, and then air-dried. The corrosion tests were performed at 1 bar total pressure. The solution was deoxygenated for at least 2 h by sparging with CO_2 before the introduction of the working electrode. After the RCE was inserted into the glass cell, a 20-min precorrosion test was conducted (Figure 5) to determine whether the initial CR was close to the blank test and to ensure no contamination from the previous test. To minimize the noise in electrochemical measurements caused by CO_2 sparging, the gas outlet of sparge tube was retracted into the headspace before injecting the CI. The headspace was purged with CO_2 throughout the test to prevent air ingress and to saturate the test solution with CO_2. The pH was adjusted by adding deoxygenated hydrochloric acid or sodium bicarbonate solution during each experiment.

The electrochemical measurements were conducted with a Gamry Reference 600† potentiostat. The CR was assessed by measuring LPR with a scan range from −5 mV_{OCP} to +5 mV_{OCP}, a scan rate of 0.125 mV/s, and a B value of 26 mV. The B value for these experiments was taken from previous research conducted on mild steel in a CO_2 environment[30] and was used in the analysis of all of the experimental data reported herein. CIs were tested at different concentrations. Each experiment was performed at least twice. CI model compounds were evaluated in the experimental conditions shown in Table 2.

RESULTS AND DISCUSSION

3.1 | Confirmation of Chemical Structures Using Spectroscopic Analysis of Products

Spectral data for each of the synthesized inhibitor model compounds are available in the Supplemental Material.

Table 1. *Composition (wt%) of Carbon Steel UNS G10180 (C1018) Corrosion Specimens*

Element	Cr	Mo	S	V	Si	C	Ni	Mn	P	Fe
Wt%	0.076	0.015	0.026	0.001	0.21	0.15	0.027	0.63	0.011	Balance

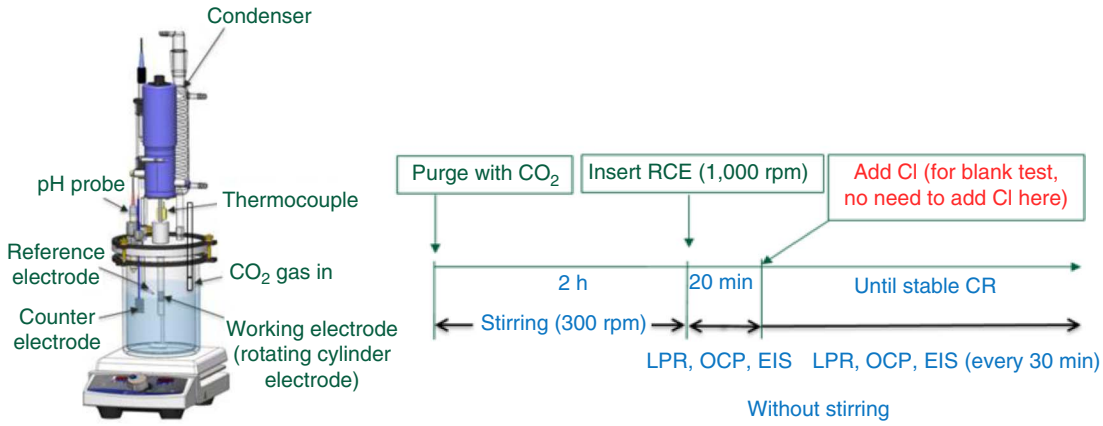

FIGURE 5. *Three-electrode setup and procedure used for corrosion experiments.*

Table 2. *Experimental Matrix for Electrochemical Experiments*

Description	Parameters
Working electrolyte	5 wt% NaCl
Material	Carbon steel UNS G10180 (C1018)
Sparge gas	CO_2
Temperature	25°C
pH	4.5±0.1
CI model compounds	1-tetradecyl-1,4,5,6-tetrahydropyrimidinium bromide (THP-C14), tetradecyl phosphate ester (PE-C14), and tetradecylimidazolinium (IMID-C14)
RCE rotating speed	1,000 rpm

For THP-C14, the NMR spectrum indicates the product is free of acetonitrile (solvent) as well as 1-bromotetradecane and tetrahydropyrimidine reactants (indicating a complete reaction). Peaks unrelated to the structure were numerically integrated to determine the level of negligible impurities (product ca. 99%+ purity).[31-33] For PE-C14, by integrating the peak area, the final product consists of 73.5% monoester and 26.5% diester. For IMID-C14, by integrating the corresponding peak area, the final product consists of imidazoline and amide and the ratio is approximately 53:47.

3.2 | Critical Micelle Concentration Measurements

3.2.1 | Determination of Critical Micelle Concentration Using Surface Tension Measurement

Figure 6 shows surface tension measurements of model inhibitor compounds THP-C14, PE-C14, and IMID-C14. With the increase in inhibitor bulk concentration in an aqueous solution, the solution/air interfacial tension decreases until it approaches a constant value at around 30 mN/m (i.e., its variation is within the measurement error), assumed to correspond to the onset of micelle formation in the bulk and termed the CMC; the intersection of the two lines in the plot of surface tension value as a function of concentration. For model inhibitor compound THP-C14 (Figure 6[a]), the intersection of the two lines for the test is between 30 ppm_w and 40 ppm_w. For model inhibitor compound PE-C14 (Figure 6[b]), the intersection of the two lines for the test is between 20 ppm_w and 30 ppm_w. For model inhibitor compound IMID-C14 (Figure 6[c]), the intersection of the two lines for the test is between 4 ppm_w and 8 ppm_w.

3.2.2 | Determination of Critical Micelle Concentration Using Fluorescence Spectroscopy

The peak emission intensity varies between CI with different concentrations. The average values of the peak emission intensities for CI with different concentrations are plotted in Figure 7. For THP-C14, from the graph (Figure 7[a]), there was an enhanced increase in emission intensity at 35 ppm_w of THP-C14 inhibitor solution, which indicates the formation of micelles in the bulk solution. The CMC of THP-C14 was determined within

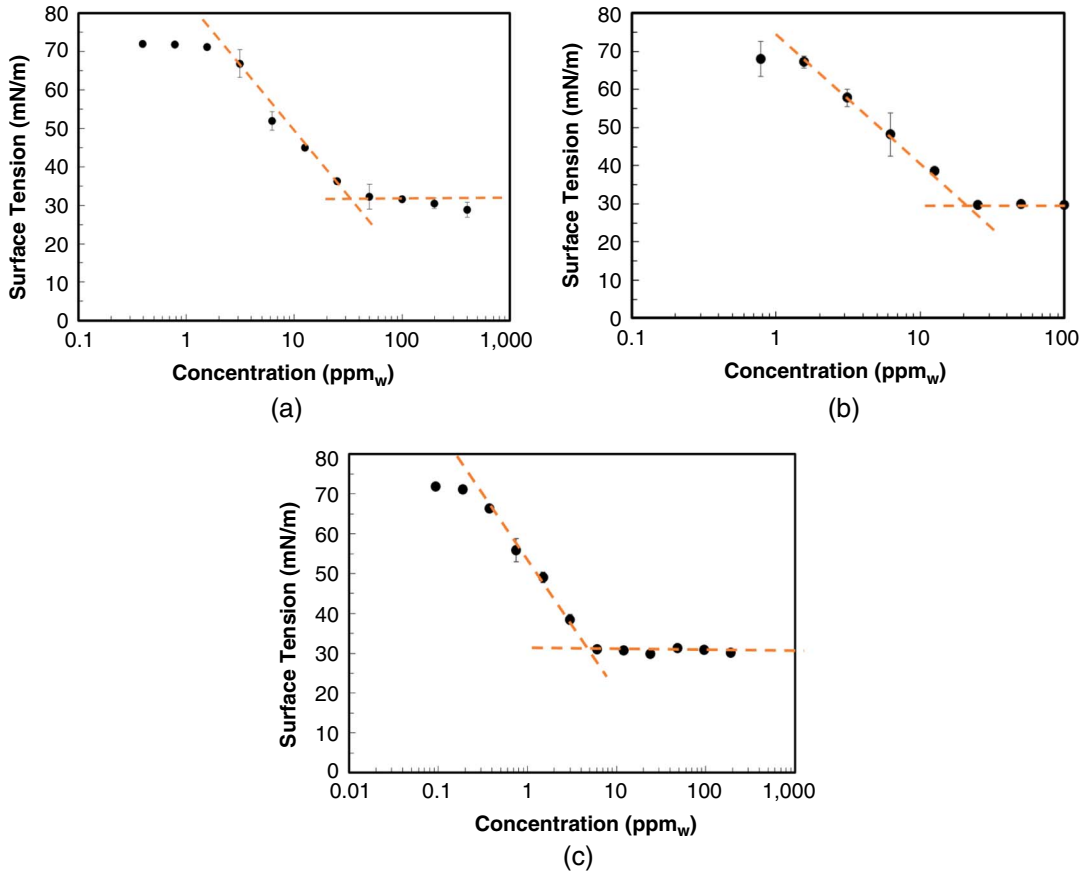

FIGURE 6. *Surface tension measurements of (a) THP-C14, (b) PE-C14, and (c) IMID-C14 model inhibitor compounds.*

the range of 17.5 ppm_w to 35 ppm_w using FS. Using the same method to analyze the data for PE-C14 (Figure 7[b]) and IMID-C14 (Figure 7[c]), the CMC value for PE-C14 in 5 wt% NaCl solution was determined within the range of 50 ppm_w to 100 ppm_w; for IMID-C14, CMC was determined within the range of 10 ppm_w to 20 ppm_w using FS.

When Moradighadi, et al., performed CMC measurements of tetradecylbenzyldimethylammonium (BDA-C14) in 1 wt% NaCl, their measured values were 50±5 ppm_w using both surface tension and FS techniques.[6,19] In the current work, the CMC values of BDA-C14[6,19] and THP-C14, although differing from each other, were each determined to be similar when measured by these different techniques. However, for PE-C14 and IMID-C14, there was a clear discrepancy between the CMC value measured by the FS and the CMC value measured using the surface tension method. This indicated that even though for BDA-C14, the value of CMC determined using surface tension measurement is close to that from FS, this does not mean that other inhibitors with the same tail length will also have CMC values determined using surface tension measurement that is close to those measured by FS.

When the CMS is reached, it is suggested that at the liquid/solid and air/liquid interfaces, the surfactants self-assemble with full coverage. Therefore, our surface tension method indirectly evaluates the micelle formation in a bulk solution via measurement at the interface between solution and air. On the other hand, FS, with respect to the determination of the CMC, is a more direct method than the Du Noüy ring method. FS facilitates characterization of the concentration and nature of amphiphilic molecules in a bulk solution, specifically whether they micellized or not, using a probe fluorophore that is encapsulated in formed micelles; here Nile Red.[25] In this view, FS is thought to be more accurate to detect the formation of micelles.

3.3 | Determination of Metal Surface Saturation Concentration

3.3.1 | Corrosion Rate Analysis

Figure 8 shows the CR of C1018 steel in the absence of an inhibitor and with various concentrations of THP-C14 in 5 wt% NaCl electrolyte at 25°C. In the absence of an inhibitor, the CR was 2.01±0.13 mm/y. In the presence of THP-C14, the CR gradually decreased with increasing inhibitor concentration from 0.25 ppm_w to 4 ppm_w. When the CI concentration was above 4 ppm_w, the CR remained low at 0.11±0.02 mm/y and relatively insensitive to further increase inhibitor concentration. The surface saturation concentration of THP-C14 in 5 wt% NaCl was determined to be within the range of 1 ppm_w to 4 ppm_w as determined from the plot of the CR as a function of time. Using the same method to analyze the data for PE-C14 and IMID-C14. Figure 9 shows the CR of C1018 steel in the absence of an inhibitor and with various concentrations of PE-C14. The MSSC of PE-C14 in 5 wt% NaCl was determined to be within the range of 2 ppm_w to 3 ppm_w, the final CR remained low to be 0.08±0.03 mm/y. Figure 10 shows the CR of C1018 steel in the absence of an inhibitor and with various concentrations of

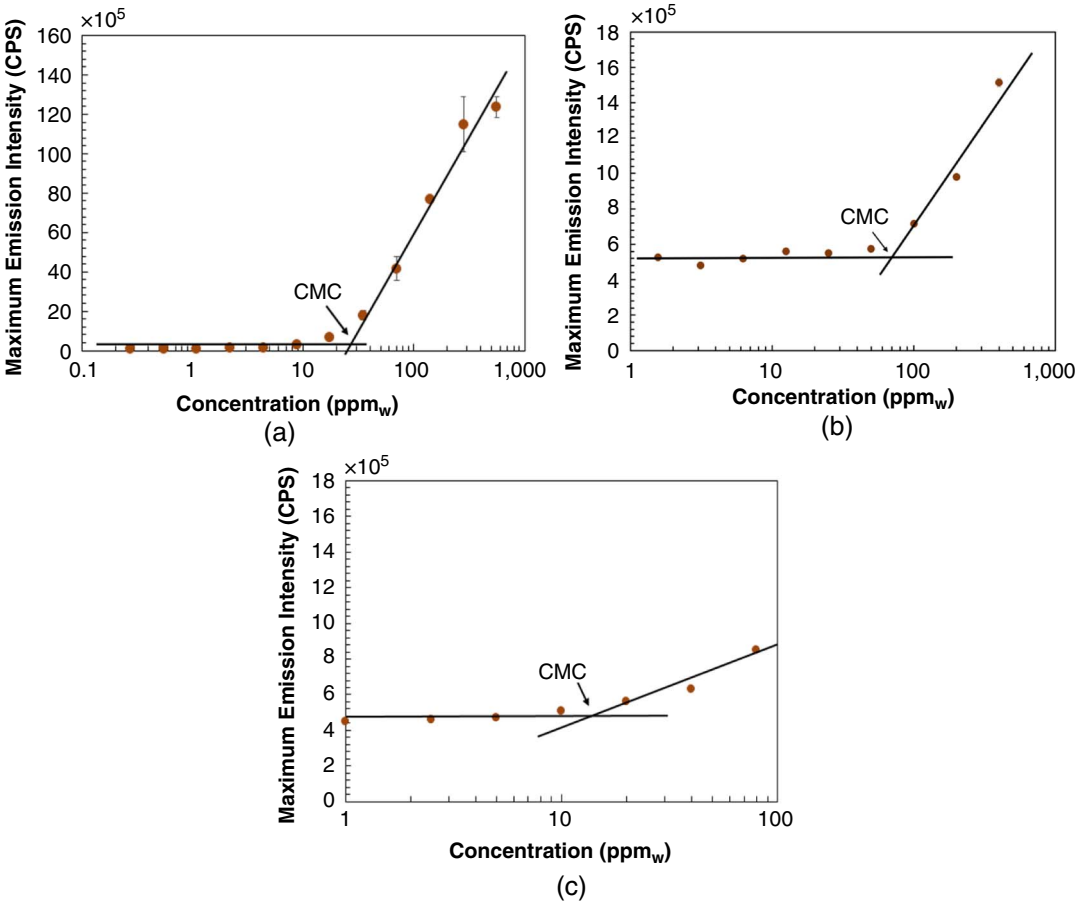

FIGURE 7. *Maximum peak emission intensities for CI (a) THP-C14, (b) PE-C14, and (c) IMID-C14 with different concentrations in 5 wt% NaCl solution.*

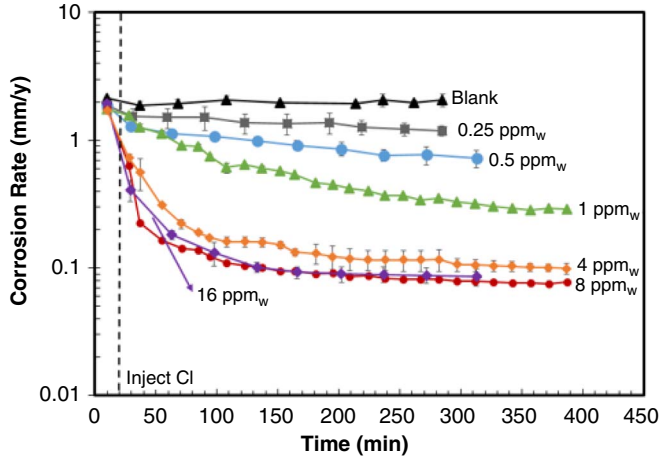

FIGURE 8. *LPR measured corrosion rates of the C1018 carbon steel immersed in 5 wt% NaCl solution in the presence and absence of THP-C14 at 25°C as a function of time.*

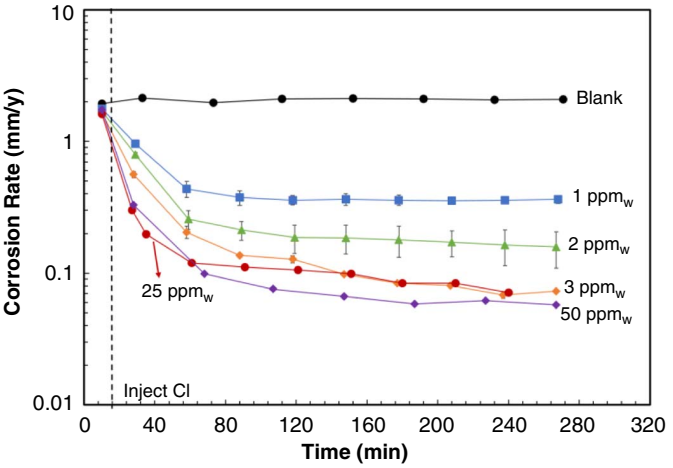

FIGURE 9. *LPR measured corrosion rates of the C1018 carbon steel immersed in 5 wt% NaCl solution in the presence and absence of PE-C14 at 25°C as a function of time.*

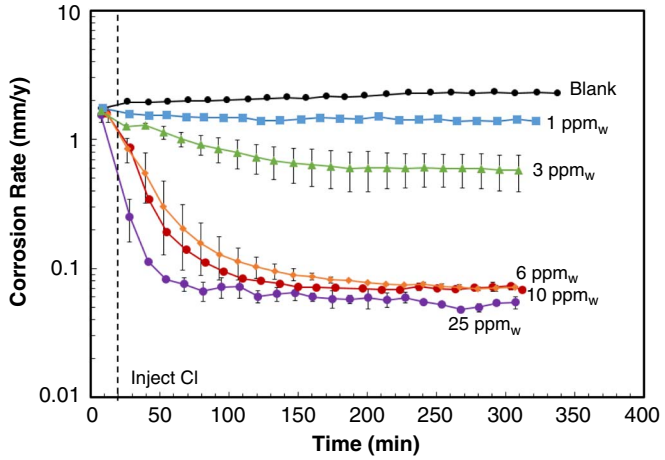

FIGURE 10. *LPR measured corrosion rates of the C1018 carbon steel immersed in 5 wt% NaCl solution in the presence and absence of IMID-C14 at 25°C as a function of time.*

IMID-C14. The metal surface saturation concentration of IMID-C14 in 5 wt% NaCl was determined to be within the range of 3 ppm_w to 6 ppm_w; bear in mind that this is present with amide in a roughly 50:50 mixture. The final CR remained low to be 0.05±0.01 mm/y.

3.3.2 | Surface Coverage Fraction (θ)

The fractional coverage (θ) of the working electrode by the CI is defined as the percentage of the substrate surface "covered" by adsorbed inhibitor molecules. Maximum or full coverage is achieved when the maximum IE has been reached (i.e., the CI concentration reaches the surface saturation value). Full or maximum coverage has a value of 1, although it does translate automatically to a low CR as some CI may have extremely low IE at full coverage. Full or maximum coverage also does not translate to a geometrical arrangement of CI molecules that leaves no free space on the substrate surface; it rather means that the free space that may exist between CI molecules is not large enough to accommodate further adsorption on the substrate surface. The fractional coverage (θ) can be calculated based on the work of Hackerman, et al.,[16] using the following equation:

$$\theta = \frac{(i_{corr})_{\theta=0} - (i_{corr})_{\theta}}{(i_{corr})_{\theta=0} - (i_{corr})_{\theta=max}} \quad (1)$$

where $(i_{corr})_{\theta=0}$ is the CR without CI, $(i_{corr})_{\theta}$ is the CR with CI, and $(i_{corr})_{\theta=max}$ is the steady-state CR with CI at the MSSC with maximum surface coverage.

The equilibrium coverage fractions for different THP-C14, PE-C14, and IMID-C14 concentrations are listed in Table 3. When the concentration is higher than MSSC, the equilibrium coverage is considered to have reached its maximum value, i.e., full coverage. Therefore, at about 8 ppm_w of THP-C14, the C1018 steel attains full coverage, while PE-C14 and IMID-C14 at 3 ppm_w and 20 ppm_w, respectively.

3.4 | Are Critical Micelle Concentrations and Inhibition Efficiencies Related?

The corrosion mitigation efficiency was calculated when the CR did not significantly decrease over time (less than ±0.01 mm/y between measurements).[18] Equation (1) was used[34-35] to calculate the corrosion mitigation efficiency (ε):

$$\varepsilon = 1 - \frac{CR_{inhibited}}{CR_{uninhibited}} \quad (2)$$

where $CR_{inhibited}$ is the steady-state CR of the system with CI and $CR_{uninhibited}$ represents the CR of the same system without the inhibitor present. Table 4 summarizes the above results of different CI model compounds. The result shows that the CIs was able to mitigate the corrosion of the C1018 steel in our experimental settings that closely simulated the conditions in the field.

Moradighadi, et al., conducted LPR CR measurements in the presence of BDA-C14 at different concentrations.[19] The MSSC in 1 wt% NaCl, pH 4.0, 30°C was determined to be within the range of 25 ppm_w to 50 ppm_w based on the maximum efficiency of the tested inhibitor; this demonstrated that the value of CMC is very close to the MSSC for BDA-C14. Interestingly, the corrosion IEs for THP-C14, PE-C14, and IMID-C14 inhibitors do not correspond with their CMC value by approximately one order of magnitude. This indicated that even though the previous result has shown that, for BDA-C14, the value of CMC is very close to the

Table 3. *The Equilibrium Coverage Fractions in Different THP-C14, PE-C14, and IMID-C14 Concentrations*

THP-C14		PE-C14		IMID-C14	
Conc. (ppm_w)	θ_{eq}	Conc. (ppm_w)	θ_{eq}	Conc. (ppm_w)	θ_{eq}
0.25	0.37	0.5	0.79	1	0.27
0.5	0.68	1	0.82	3	0.77
1	0.89	1.5	0.90	6	0.97
4	0.96	2	0.93	10	0.99
8	1	3	1	20	1
16	1	25	1	40	1

Table 4. *Parameters of CI Model Compounds*

Type of Inhibitor	CMC Value by FS (ppm_w)	Metal Surface Saturation Concentration (ppm_w)	Steady State Inhibited CR (mm/y)	Inhibition Efficiency (%)
THP-C14	17.5–35	1–4	0.11±0.02	95
PE-C14	50–100	2–3	0.08±0.03	95
IMID-C14	10–20	3–6	0.05±0.01	97
BDA-C14[(A)]	50±1	25 –50	0.22±0.04	93

[(A)] See Moradighadi, et al.,[6,19] for sources of data.

MSSC, this does not mean that other inhibitors with different headgroups with the same tail length C14 will also have CMC values that are close to the MSSC. The surface tension and FS measurements used for most CMC evaluations are conducted at the air/solution interface or in bulk solution, which may not necessarily have a direct relationship to the inhibitor coverage at the metal/solution interface.[6] Consequently, these results further demonstrate that there is no generalizable direct link between CMC and surface coverage, and by extension to corrosion IE. The optimal inhibitor concentration used in a pipeline should be chosen based on the actual corrosion IE, instead of the CMC.[36] CMC alone is not enough to state the optimal efficiency of a given CI. Besides, CMC values for the tested CI model compounds are all greater than the values obtained from performing the CR analysis (MSSC). It is more economical (usage of CIs) to know the CR rather than basing the concentrations on CMC measurement. Although some CIs may function well below their CMC value,[37] this concentration could still be a good starting point for testing, i.e., start testing at CMC, and if it works at this concentration, explore what happens as the concentration is decreased. Furthermore, the maximum corrosion IE is 97%, which means that the corrosion cannot become fully inhibited/stopped; corrosion will always happen, albeit mitigated. In practice, this residual CR is of great interest to operators. As mentioned earlier, this discussion only applies to bare metal surfaces. The presence of corrosion products or residues ($FeCO_3$, Fe_xS_y, Fe_3C, and Fe_xO_y) may lead to situations where a different inhibitor dosage is required. In all cases, the value of CMC would still bear no relevance to the extent of corrosion inhibition.

CONCLUSIONS

➢ This work presents the development and application of a methodology for CI characterization and inhibition evaluation to three model compounds with different head groups but the same alkyl tail length ($-C_{14}H_{29}$): tetradecyltetrahydropyrimidinium (THP-C14), tetradecylphosphate ester (PE-C14), and tetradecylimidazolinium (IMID-C14). The CMCs of each compound were measured using surface tensiometry (Du Noüy ring) and FS techniques. The result indicated that even though for BDA-C14 the value of CMC determined using surface tension measurement is close to that using FS, this does not mean that other inhibitors with the same tail length C14 will also have CMC values determined using surface tension measurement is close to that use FS. CR measurements over various CI concentrations yielded MSSC values for each model compound. The CI performance can be assessed by IE (calculated from CR), with MSSC serving as practical dosing guidance. These results are crucial and practical in oil and gas industry applications. Ongoing research focuses on the domain of validity of the inhibition model for these model compounds. Although coverage of a metal surface by inhibitor molecules is considered a barrier against corrosive species, the actual mechanism of protection is not akin to a solid impenetrable layer being present.

➢ Regarding the effect of the alkyl tail length of the CIs, there have been studies relating the alkyl tail with the mitigation efficiency of the CIs.[38-40] In those studies, corrosion efficiency and/or changes in the double layer capacitances were measured. Measurements were integrated into mathematical models based upon adsorption isotherms assuming that the coverage of the inhibitor on the metal surface (θ) is proportional to the corrosion mitigation efficiency.[8,41] In general, it was concluded that the longer the CI alkyl tail, the greater the corrosion mitigation efficiency. However, the key link between the inhibitor head group (with the same alkyl tail length) and surface coverage is not properly established. From the above results, it is shown that IMID-C14 had a higher corrosion IE than the other inhibitors. This can be postulated to be due to the way that the inhibitor is adsorbed on the surface, which depends on the size and the type of the head group and the bonding between alkyl tails which enhances inhibitor film stability. Further research is ongoing to address questions relating to how a CI diminishes corrosion, including establishing the mechanistic role the head group plays on the processes involved, as they are not fully answered; temperature, corrosion products, and brine effects are also under investigation.

In summary:

➢ Three CI model compounds with different head groups but the same alkyl tail length ($-C_{14}H_{29}$), specifically tetradecyltetrahydropyrimidinium (THP-C14), tetradecylphosphate ester (PE-C14), and tetradecylimidazoline (IMID-C14), were synthesized. Their purities are determined using NMR.

➢ CMC values were obtained by metal surface tension measurements and FS, with differences found between these indirect and direct methods. The corrosion IEs for THP-C14, PE-C14, and IMID-C14 inhibitors do not correspond with their CMC value. FS, with respect to the determination of the CMC, seems to be a more direct measurement technique than the Du Noüy method.

➢ The MSSC of THP-C14, PE-C14, and IMID-C14 were determined to be 1 ppm_w to 4 ppm_w, 2 ppm_w to 3 ppm_w, and 3 ppm_w to 6 ppm_w, respectively; their IEs were 95%, 95%, and 97%.

➢ The correlation between CMC and IE was achieved by comparing the corrosion inhibition parameters for the same inhibitor. Results indicate that for CI model compounds with the different head groups but the same alkyl tail length ($-C_{14}H_{29}$), there is no direct link between CMC and surface coverage, and by extension to corrosion IE. CMC alone is consequently not an accurate indicator to assess the performance or the needed dosage of a given CI—in some cases, it can be completely misleading and lead to the requirement of a higher dosage.

ACKNOWLEDGMENTS

This project has been supported by TotalEnergies transversal R&D project (MANA Project). The authors would like to thank TotalEnergies for their financial support and valuable discussions. Prof. Klaus Himmeldirk from Ohio University is thanked for the discussion of the synthesis of THP-C14 and for supplying Figure 2.

References

1. M.B. Kermani, D. Harrop, *SPE Prod. Facil.* 11 (1996): p. 186-190.
2. Y. Xiong, B. Brown, B. Kinsella, S. Nešić, A. Pailleret, *Corrosion* 70 (2014): p. 247-260.
3. Y. Duda, R. Govea-Rueda, M. Galicia, H.I. Beltraén, L.S. Zamudio-Rivera, *J. Phys. Chem. B* 109 (2005): p. 22674-22684.
4. Y. Ding, B. Brown, D. Young, M. Singer, "Effectiveness of an Imidazoline-Type Inhibitor against CO_2 Corrosion of Mild Steel at Elevated Temperatures (120°C–150°C)," CORROSION 2018, paper no. 11622 (Houston, TX: NACE, 2018).
5. Z. Belarbi, T.N. Vu, F. Farelas, D. Young, M. Singer, S. Nešić, *Corrosion* 73 (2017): p. 892-899.
6. N. Moradighadi, S. Lewis, J.M. Domínguez Olivo, D. Young, B. Brown, S. Nešić, *Corrosion* 77 (2021): p. 266-275.
7. J.M. Domínguez Olivo, "Electrochemical Model of Carbon Dioxide Corrosion in the Presence of Organic Corrosion Inhibitors" (Ph.D. diss., Ohio University, 2020).
8. V.S. Sastri, *Green Corrosion Inhibitors, Green Corrosion Inhibitors: Theory and Practice* (Hoboken, NJ: John Wiley & Sons, Inc., 2011).
9. S. Sharma, X. Ko, Y. Kurapati, H. Singh, S. Nešić, *Corrosion* 75 (2019): p. 90-105.
10. M.A. Malik, M.A. Hashim, F. Nabi, S.A. AL-Thabaiti, Z. Khan, *Int. J. Electrochem. Sci.* 6 (2011): p. 1927-1948.
11. M.L. Free, *Corros. Sci.* 44 (2002): p. 2865-2870.
12. IUPAC, "Critical Micelle Concentration," *Compendium of Chemical Terminology*, 2nd ed. (Research Triangle Park, NC: International Union of Pure and Applied Chemistry (IUPAC), 1997).
13. K. Nesměrák, I. Němcová, *Anal. Lett.* 6 (2006): p. 1023-1040.
14. S. Ebnesajjad, "Material Surface Preparation Techniques," *Handbook of Adhesives and Surface Preparation (William Andrew Publishing,* 2011), p. 49-81.
15. S. Thomas, R. Thomas, A.K. Zachariah, R.K. Mishra, *Thermal and Rheological Measurement Techniques for Nanomaterials Characterization* (Amsterdam, Netherlands: Elsevier, 2017).
16. T. Murakawa, S. Nagaura, N. Hackerman, *Corros. Sci.* 7 (1967): p. 79-89.
17. M. El Achouri, Y. Bensouda, H.M. Gouttaya, B. Nciri, L. Perez, M.R. Infante, *Tenside Surfactants Deterg.* 38 (2001): p. 208-215.
18. J.M. Domínguez Olivo, B. Brown, D. Young, S. Nešić, "Electrochemical Model of CO_2 Corrosion in the Presence of Quaternary Ammonium Corrosion Inhibitor Model Compounds," CORROSION 2019, paper no.13392 (Houston, TX: NACE, 2019).
19. N. Moradighadi, S. Lewis, J.M. Domínguez Olivo, D. Young, B. Brown, S. Nešić, "Effect of Alkyl Tail Length on CMC and Mitigation Efficiency Using Model Quaternary Ammonium Corrosion Inhibitors," CORROSION 2019, paper no.13004 (Houston, TX: NACE, 2019).
20. J.M. Domínguez Olivo, D. Young, B. Brown, S. Nešić, "Effect of Corrosion Inhibitor Alkyl Tail Length on the Electrochemical Process Underlying CO_2 Corrosion of Mild Steel," CORROSION 2018, paper no. 11537 (Houston, TX: NACE, 2018).
21. S. Patai, *Chemistry of the Amino Group* (Hoboken, NJ: Wiley-Interscience, 1968), p. 45-52.
22. H.Z. Sommer, H.I. Lipp, L.L. Jackson, *J. Org. Chem.* 36 (1971): p. 824-828.
23. Y. Shi, Y. Zhao, G. Zhang, Q. Dong, *Tenside Surfactants Deterg.* 56 (2019): p. 244-251.
24. J.A. Martin, F.W. Valone, *Corrosion* 41 (1985): p. 281-287.
25. P. Greenspan, S.D. Fowler, *J. Lipid Res.* 26 (1985): p. 781-789.
26. A.M. Peterson, Z. Tan, E.M. Kimbrough, J.M. Heemstra, *Anal. Meth.* 7 (2015): p. 6877-6882.
27. J.M. Neugebauer, *Meth. Enzymol.* 182 (1990): p. 239-253.
28. Y. Liang, Y. Sun, X. Fu, Y. Lin, Z. Meng, Y. Meng, J. Niu, Y. Lai, Y. Sun, *Artif. Cells, Nanomed. Biotechnol.* 48 (2020): p. 525-532.
29. R.P.W.M. Jacobs, R.O.H. Grant, J. Kwant, J.M. Marquenie, E. Mentzer, *The Composition of Produced Water from Shell Operated Oil and Gas Production in the North Sea in Produced Water* (Boston, MA: Springer US, 1992), p. 13-21.
30. Z. Belarbi, F. Farelas, M. Singer, S. Nešić, *Corrosion* 2 (2016): p. 1256-1270.
31. R.M. Silverstein, G.C. Bassler, T.C. Morrill, *Spectrometric Identification of Organic Compounds, Organic Mass Spectrometry*, 5th ed. (New York, NY: Wiley, 1991).
32. Nmrdb.org, "Tools for NMR Spectroscopists" (n.d.), http://www.nmrdb.org/.
33. D. Whittaker, *Interpreting Organic Spectra* (Piccadilly, United Kingdom: Royal Society of Chemistry, 2007).
34. S. Papavinasam, Evaluation and Selection of Corrosion Inhibitors, in *Uhlig's Corrosion Handbook*, 3rd ed. (Hoboken, NJ: John Wiley and Sons, 2011), p. 1121-1127.
35. E. McCafferty, *Introduction to Corrosion Science* (New York, NY: Springer, 2010).
36. Y. He, S. Ren, Z. Belarbi, X. Wang, D. Young, M. Singer, M. Mohamed-Saïd, C. Sheyla, "Micellization and Inhibition Efficiency," CORROSION 2021, paper no. 16872 (Houston, TX: AMPP, 2021).
37. K. Kousar, M.S. Walczak, T. Ljungdahl, A. Wetzel, H. Oskarsson, P. Restuccia, E.A. Ahmad, N.M. Harrison, R. Lindsay, *Corros. Sci.* 180 (2021): p. 109195.
38. A. Edwards, C. Osborne, S. Webster, D. Klenerman, M. Joseph, P. Ostovar, M. Doyle, *Corros. Sci.* 36 (1994): p. 315-325.
39. D. Asefi, M. Arami, A.A. Sarabi, N.M. Mahmoodi, *Corros. Sci.* 51 (2009): p. 1817-1821.
40. E. McCafferty, N. Hackerman, *J. Electrochem. Soc.* 119 (1972): p. 146.
41. L.M. Vračar, D.M. Draži, *Corros. Sci.* 44 (2002): p. 1669-1680.